

ORIGINAL ARTICLE

Laser Machining of Die Steel (EN-31): An Experimental Approach to Optimise Process Parameters using Response Surface Methodology

A.R. Patel¹ and S.N. Bhavsar²¹Chandubhai S Patel Institute of Technology, CHARUSAT, Changa, Gujarat, India – 388421
Phone: 7600010215²Mechatronics Department, G H Patel College of Engineering and Technology, Vallabh Vidyanagar, Gujarat, India -388120

ABSTRACT – Experiments were performed based on response surface methodology (RSM) to investigate the process parameters effect on the features of hole geometry. Cutting speed (of 500-1000 mm/min), laser power (of 2000-4000 W), frequency (of 800-2000 Hz), duty cycle (of 75-95%), and gas pressure (of 0.05-0.15 bar) were considered as variable parameters. Deviation in the dimension of entrance and exit holes, heat affected zone (HAZ) on the upper & lower edge, and roughness were the output to analyse the cutting quality of 14 mm thick normal and heat-treated (HT) EN-31 die steel using 4 kW CO₂ laser. For untreated plate, minimum taper angle was achieved with low cutting speed, higher laser power, and gas pressure. Higher cutting speed, low laser power, and higher gas pressure result in the minimum HAZ. For the HT plate, the mid-range of parameters results in the minimum taper angle and HAZ. An optimised model was developed, and the confirmatory test gives roughness up to 0.27 microns and it shows good agreement with the mathematical model. At the cross-section of holes, striation pattern, resolidified layer, and corner qualities were visually inspected. Surface damage near the cutting edge was observed using scanning electron microscopy.

ARTICLE HISTORYReceived: 8th Sept 2020Revised: 7th Dec 2020Accepted: 5th Jan 2021**KEYWORDS***Laser machining;**Optimisation;**RSM;**Surface roughness;**HAZ***NOMENCLATURE**

- Y response of empirical model
 X_1 cutting speed
 X_2 laser power
 X_3 frequency
 X_4 duty cycle
 X_5 gas pressure

INTRODUCTION

Greater competitiveness is found in today's metal processing industries. Productivity, accuracy, non-contact machining, less use of energy with good surface quality and use of advanced engineering materials like titanium and its alloys, steel and its alloy, nickel-based superalloys, ceramics and composites with complicated shapes and unusual size of the workpiece restrict the use of traditional machining. The laser applies to almost all materials from the metallic to the non-metallic range and is used for cutting, marking, drilling, welding, melting and sintering [1-4]. Different lasers like CO₂, Nd-YAG, fibre and excimer are available; a plate with a larger thickness (of more than 8-10 mm) can be cut by CO₂ laser with a higher cutting speed. Hence, the CO₂ laser is widely used in the structural components, medical industries, automotive parts, aircraft, die making, and many more medium scale industries [5-9]. Process parameters like laser power, cutting speed, frequency, duty cycle, gas pressure, pulsed or continuous mode of operation, focal point position and nozzle diameter vary from material to material and need to be optimised for getting the desired output with minimum defects. Generally, defects like resolidification of the molten material on layers, dross adhesion, oxidation of the surface, heat-affected zones, and improper flatness found on the cut surfaces [10-15].

Molian compared the cutting quality of hard to machine material using a single beam and dual beam of 1.5 kW CO₂ laser. The author concluded that it could be possible to cut material at a higher speed using a dual-beam without losing cutting quality [16]. Mushtaq et al. reviewed the cutting application of CO₂ laser in the different types of polymeric materials. The author discussed the effect of process parameters such as laser power, cutting speed, assist gas pressure, pulse frequency, nozzle type and its diameter, stand-off distance on the output responses like heat affected zone (HAZ), roughness, kerf width, dross, and striation formation [17]. Golyshhev presented data of surface roughness for 3 mm, 5 mm, 8 mm, and 10 mm thick low carbon steel sheets for both conditions of laser beam polarisation. i.e. circular polarisation

and plane polarisation. The author found that better surface roughness reached when the direction of cutting speed is perpendicular to the polarisation plane [18]. Hossain et al. built a model based on a fuzzy expert system to forecast the kerf width of CO₂ laser cutting using MATLAB on a 3 mm thick polymethyl-methacrylate sheet and validate model accuracy with the experimental run [19]. Seong et al. compared melt cutting efficiency of 60 mm thick steel plate based on interferometric analysis by using two different nozzle geometry with different stand-off distances and concluded that supersonic nozzle could be the proper approach for higher cutting efficiency [20].

Genna et al. discussed the cutting quality of AISI 304 stainless steel, St37-2 low carbon steel, and AlMg3 aluminium alloy with variable thickness by analysing the kerf width, roughness, and cut edge quality. The author concluded that thickness affects the top kerf width, while bottom kerf width is governed by gas pressure. Roughness influenced by the interaction of material type and cutting speed [21]. Moradi and Abdollahi investigated the hole geometrics features for thin SS 321 sheet using the design of experiments and concluded with minimum taper angle with an increase in the pulse frequency and decrease in the laser power. The author generated the optimised model for minimum hole taper and verified it with experiments [22]. Literature survey concluded that the limited research available on CO₂ laser cutting for hard and thick alloy steel using oxygen as an assisted gas [23, 24].

The die industry often requires holes to be cut in thick and hard plates, and problems reported regarding the cutting qualities achieved by conventional cutting technology. With this context, the objective of this research is to analyse and compared the effect of process parameters for CO₂ laser cutting on untreated and heat-treated (HT) plates. Response surface methodology (RSM) has been applied to reduce the number of experiments and to get a quadratic mathematical equation that relates the input and output parameters logically. Individual, square and interaction effects of parameters were identified, and a good agreement of experimental results with the mathematical model for each response. An optimised model was generated, and significant parameters were identified to minimise the responses; taper angle, HAZ and roughness. Surface damage or micro-cracks near the cutting edges were observed using scanning electron microscopy.

MATERIALS AND METHODOLOGY

One factor at a time, Taguchi and the two-level factorial design are not able to estimate the quadratic effect and interaction effect. So, a three-level design of experiment (DOE) was used with RSM–centre composite design (CCD) for the experiments [25-27]. Die alloy steel EN 31 have been selected due to its utility demand in different products, like axels, heavy-duty gears, camshafts, gudgeon pins, driving pinion and link, components for transportation and energy products, roller bearings, ball bearings, shear blades, spindle, forming and moulding dies, beading rolls, punches and dies. Two plates of 300 mm × 150 mm with 14 mm thickness have been prepared, one with a normal hardness and another with a higher hardness. The hardness of EN-31 material, initially measured as 22 HRC. To understand the effect of laser cutting on the hard material, a heat treatment process has been carried out using brine solution by quenching process. As a result, hardness increased to 58 HRC. Table 1 shows the chemical composition of EN-31.

Table 1. Chemical composition and hardness of EN-31 Die-steel sample.

%C	%Si	%Mn	%P	%S	%Cr	Before heat treatment	After heat treatment
0.94	0.14	0.469	0.05	0.06	1.064	22 HRC	58 HRC

AMADA AF4000i-B CO₂ laser machine with 4000W was used for the experiment. A positive focal plane position of 1 mm has been set for holes cutting, as per the machine manufacturer catalogue. The range of the parameters identified through the initial experiments and the limits of the parameters are shown in Table 2.

Statistical software, Minitab V16, was used to prepare the design matrix. Table 3 shows the value of the parameter for 27 experiments based on RSM-CCD. Statistical and response plots, as well as optimisation, have been carried out to meet the requirements of the die industry. Here, RSM is selected because of its capacity to measured significant interaction effect of parameters and expressed as a function of X_1, X_2, etc . Quadratic polynomial functions have been identified as per Eq. (1) for all the responses using RSM.

$$Y = b_0 + b_1X_1 + b_2X_2 + \dots + b_{11}X_1^2 + b_{22}X_2^2 + \dots + b_{12}X_1X_2 + b_{n-1,n}X_{n-1}X_n \quad (1)$$

where Y is a response, X_i is process parameters and b_i is a regression coefficient.

Table 2. List of the parameter with their notation, unit and levels.

Process parameters	Notation	Unit	Level 1	Level 2	Level 3
Cutting speed	X_1	mm/min	500	750	1000
Laser power	X_2	Watt	2000	3000	4000
Frequency	X_3	Hz	800	1400	2000
Duty cycle	X_4	%	75	85	95
Gas pressure	X_5	bar	0.05	0.1	0.15

Table 3. Experimental runs according to central composite design (RSM-CCD).

Run	Cutting speed (mm/min)	Power (W)	Frequency (Hz)	Duty cycle (%)	Gas pressure (bar)
1	500	2000	2000	75	0.05
2	750	3000	1400	95	0.1
3	1000	3000	1400	85	0.1
4	750	3000	2000	85	0.1
5	1000	2000	800	75	0.05
6	750	3000	800	85	0.1
7	500	2000	2000	95	0.15
8	1000	2000	800	95	0.15
9	500	2000	800	95	0.05
10	750	2000	1400	85	0.1
11	500	4000	800	95	0.15
12	500	4000	2000	75	0.15
13	500	2000	800	75	0.15
14	500	3000	1400	85	0.1
15	750	4000	1400	85	0.1
16	500	4000	2000	95	0.05
17	1000	4000	800	95	0.05
18	1000	4000	800	75	0.15
19	750	3000	1400	75	0.1
20	750	3000	1400	85	0.05
21	1000	4000	2000	95	0.15
22	1000	4000	2000	75	0.05
23	1000	2000	2000	75	0.15
24	500	4000	800	75	0.05
25	1000	2000	2000	95	0.05
26	750	3000	1400	85	0.15
27	750	3000	1400	85	0.1

RESULTS AND DISCUSSION

Figure 1 shows the position of 27 holes cut on a 14 mm thick EN-31 plate from the top and bottom view for both untreated and HT plates. Rectangular holes of 10 mm × 20 mm have been cut, and the distance between two successive holes have been kept at a sufficient distance apart to avoid overlapping of HAZ. In the industry, it has been observed that, when cutting thick material, the bottom edge dimensions changed from the original required dimensions. The tapered effect was calculated by measuring the hole dimensions on the top and bottom edge using Eq. (2).

$$\text{Taper angle } (\theta) = \frac{(\text{hole dimension at top edge} - \text{hole dimension at bottom edge})}{2 \times \text{Thickness of plate}} \quad (2)$$

HAZ were measured on the top, and bottom edge of plates by using Mitutoyo make 3D microscope, model QS-L2010ZB, with 4× zoom capacity and a 0.1 m resolution. The roughness value measured were non-identical at different depths. Surface roughness on the cutting edges has been measured using the Surfest SV2100 Colum type surface roughness tester. The sampling length of 10 mm for each measurement has been kept constant. A total of three readings have been measured along with the depth of cut, at the top, middle and bottom edge of the plate thickness. Out of these three, the maximum roughness value has been selected for further analysis of minimising the roughness. Table 4 comprises the experimental results for taper angle, HAZ, and surface roughness.



(a)



(b)



Figure 1. Position of holes from the (a) top view of the untreated plate, (b) bottom view of the untreated plate, (c) top view of HT plate and (d) bottom view of HT plate.

It is not possible to measure the taper angle and surface roughness for hole number 5 as it was not cut properly. It may happen because the laser beam energy was not enough to pass through the thickness, and the melt was not extracted perfectly due to an improper combination of the process parameter.

Table 4. Experimental results for taper angle, HAZ and surface roughness.

Run	Taper angle (°)		HAZ (top) (mm)		HAZ (bottom) (mm)		Ra (µm)	
	Untreated	HT	Untreated	HT	Untreated	HT	Untreated	HT
1	1.37	1.45	0.38	0.32	6.87	0.94	6.15	7.10
2	1.10	0.80	0.48	0.35	2.17	1.04	4.22	5.95
3	1.13	1.17	0.36	0.31	2.79	1.54	3.16	3.74
4	1.07	0.91	0.58	0.21	2.42	1.12	4.00	5.21
5	-	1.38	0.44	1.17	5.82	2.77	-	2.99
6	0.92	0.76	0.51	0.18	2.68	1.47	4.98	5.26
7	0.44	0.78	0.50	0.17	2.53	1.34	7.10	9.98
8	1.12	0.66	0.32	0.14	3.98	1.56	3.29	4.01
9	1.32	1.46	0.86	0.18	7.46	2.52	5.98	7.33
10	1.33	1.16	0.73	0.19	4.55	1.82	4.32	6.69
11	0.27	1.12	0.62	0.23	2.63	1.69	7.00	8.21
12	0.07	0.98	1.73	0.17	3.24	1.84	5.82	12.1
13	0.90	1.14	0.54	0.12	3.61	2.08	6.72	10.4
14	0.55	0.90	0.56	0.23	3.71	1.31	6.94	9.26
15	0.76	1.06	0.91	0.25	2.8	1.84	4.60	8.88
16	1.22	1.18	1.07	0.98	5.78	2.16	8.17	10.2
17	1.15	1.38	0.73	0.21	4.12	2.36	2.77	4.16
18	1.06	1.28	0.52	0.41	2.23	2.45	3.27	3.49
19	1.10	0.69	0.54	0.55	3.02	1.24	4.37	5.72
20	1.30	1.29	0.62	0.87	5.92	1.98	4.04	3.98
21	1.10	1.27	0.44	1.01	2.89	2.15	3.38	3.63
22	1.33	1.13	0.79	0.13	3.88	1.92	2.27	3.04
23	1.17	1.26	0.46	0.97	3.57	1.97	3.96	3.80
24	1.09	1.38	0.68	0.99	6.88	2.11	6.32	9.29
25	1.35	1.41	0.65	0.20	5.85	3.46	2.73	2.71
26	0.90	1.14	0.45	0.65	4.26	2.08	4.53	5.36
27	0.93	0.96	0.50	0.39	2.69	1.58	4.71	5.52

Effect of Process Parameters on Taper Angle

The main effect plot for the taper angle has been developed, as shown in Figure 2. The taper angle presents in almost all cases of thick and hard material because of beam penetration characteristics. At higher cutting speed, the laser beam did not concentrate on the single point and not able to generate the required heat energy, and hence it created the taper in the untreated plate. For the HT plate, a better taper angle was achieved at the intermediate cutting speed of 750 mm/min. Higher laser power helps to penetrate the laser beam to the bottom edge and able to cut the hole properly. But, at the higher laser power of 4000 W, the taper angle increased. It might occur due to material property and the reaction of molecules with the higher heat intensity of the laser beam. The frequency and duty cycle seems less significant, according to the main effect plot. High gas pressure leads to a lower taper angle for the untreated plate because higher pressure helps the molten kerf extract rapidly from the kerf space. For the HT plate, initially, the taper angle reduced, but at 0.15 bar gas pressure, a higher taper angle was achieved. It is commonly observed for the HT plate that at both extreme positions, taper angle achieved higher compared to the untreated plate.

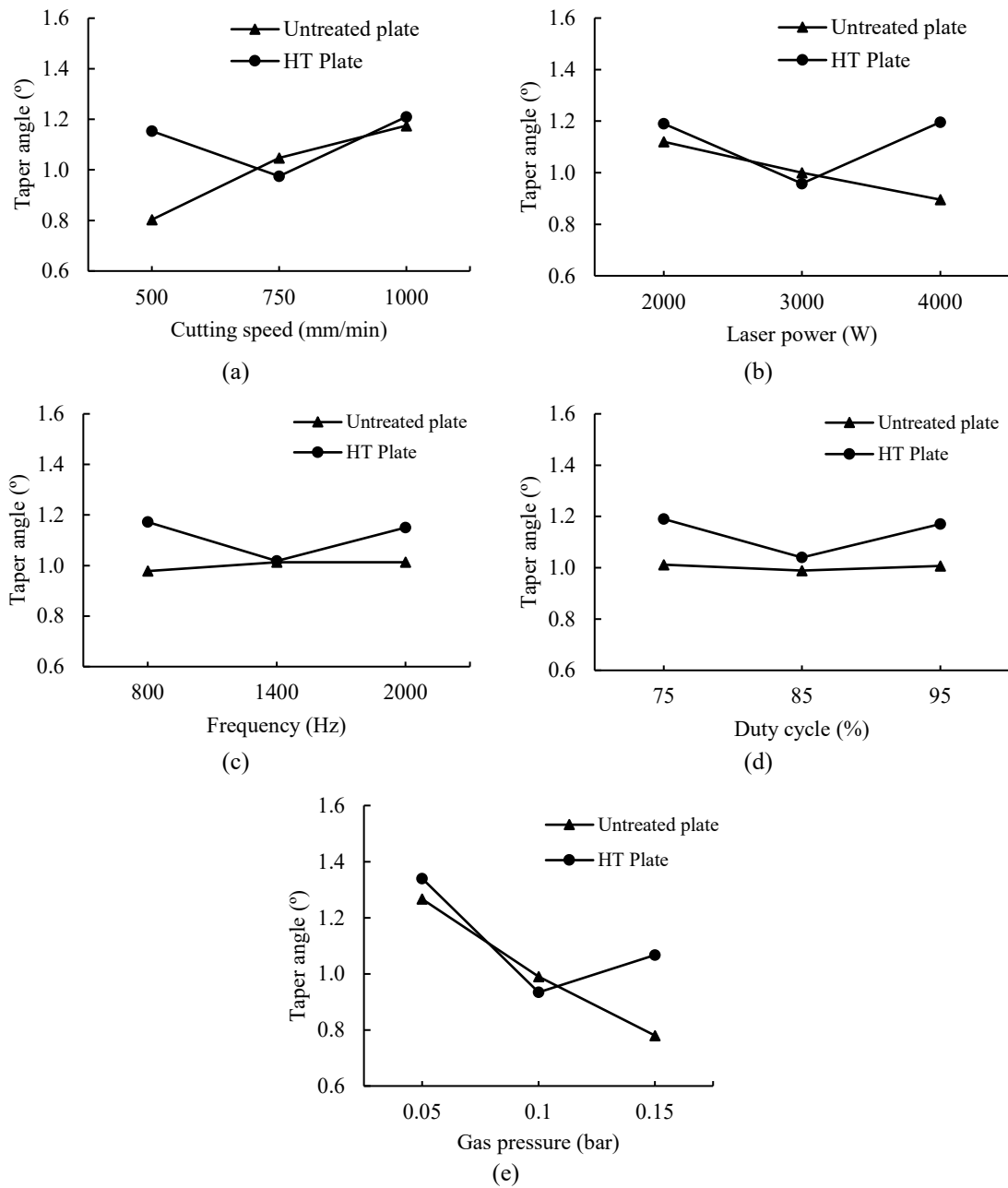


Figure 2. Main effect plot for taper angle with respect to (a) cutting speed, (b) laser power, (c) frequency, (d) duty cycle and (e) gas pressure.

Figure 3 illustrates the response surface plot for the taper angle to understand the interaction effect. Figure 3(a) depicts that the mid-value of the gas pressure and laser power lead to a minimum taper angle for the HT plate. In Figure 3(b), the higher frequency and minimum cutting speed give a minimum taper angle. A mathematical model for taper angle has been developed with regression coefficient R^2 was 96% and 95% for the untreated and HT plate, respectively, as shown in Eq. (3) and (4).

$$\begin{aligned}
 Y_{(Taper\ angle-Untreated)} &= 13.25 + 0.005 X_1 - 0.0011 X_2 - 0.0014 X_3 - 0.2 X_4 - 25.1 X_5 - 2.5 \times 10^{-6} X_1^2 \\
 &+ 0.001 X_4^2 + 41.83 X_5^2 + 1.13 \times 10^{-7} X_1 X_2 - 1.45 \times 10^{-5} X_1 X_4 + 0.01 X_1 X_5 \\
 &+ 1.14 \times 10^{-7} X_2 X_3 + 8.4 \times 10^{-6} X_2 X_4 + 1.34 \times 10^{-5} X_3 X_4 - 7.37 \times 10^{-4} X_3 X_5 \\
 &+ 0.05 X_4 X_5
 \end{aligned} \tag{3}$$

$$\begin{aligned}
 Y_{(Taper\ angle-HT)} &= -6.65 - 0.0035 X_1 - 0.0018 X_2 + 0.0002 X_3 + 0.3 X_4 - 24.4 X_5 + 1.55 \times 10^{-6} X_1^2 \\
 &+ 1.74 \times 10^{-7} X_2^2 - 2.76 \times 10^{-7} X_3^2 - 0.0019 X_4^2 + 112 X_5^2 + 1.28 \times 10^{-7} X_1 X_2 \\
 &+ 4.5 \times 10^{-7} X_1 X_3 + 0.003 X_1 X_5 - 8.89 \times 10^{-8} X_2 X_3 + 6.9 \times 10^{-6} X_2 X_4 + 0.0017 X_2 X_5 \\
 &+ 3.97 \times 10^{-6} X_3 X_4 + 0.001 X_3 X_5 - 0.116 X_4 X_5
 \end{aligned} \tag{4}$$

Experimental results have been compared with the mathematical model and found a very good agreement between these two results.

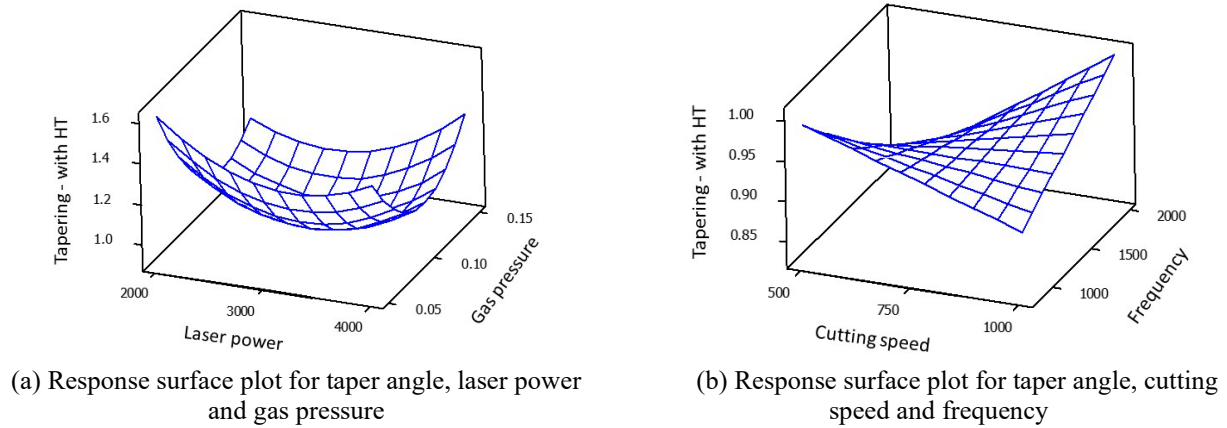


Figure 3. Response surface plot for the taper angle.

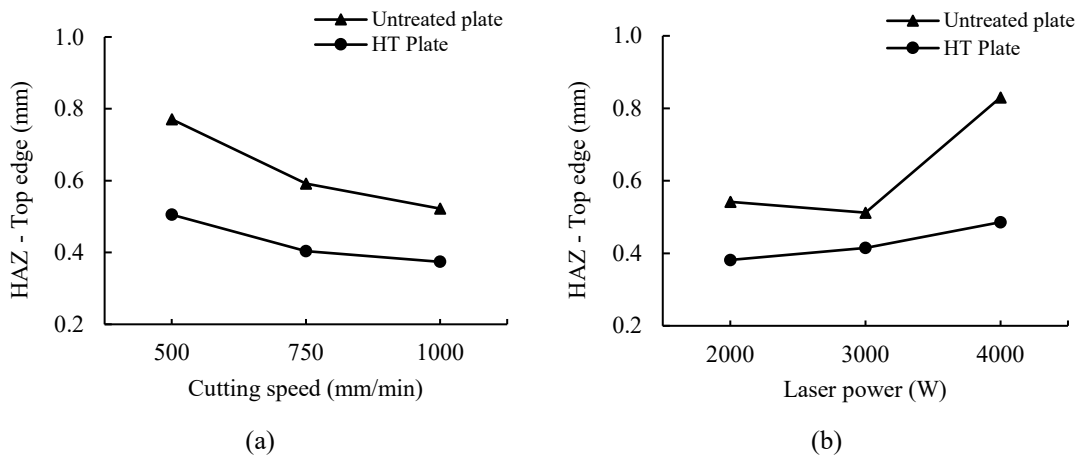
Effect of Process Parameters on Heat Affected Zone

For the untreated plate, HAZ on the top and bottom edge was visible, but the same was not true for the HT plate. In the untreated plate, the bottom edge has more HAZ compared to the top edge due to the bottom edge cut at the last, and melt took longer time to extract from the kerf and a chance to stick at the bottom edges, known as dross. Figure 4 shows the main effects plots for HAZ of the top edge for the untreated and HT plates.

It shows that the higher cutting speed leads to a lesser HAZ on the top edge for both plates because at any time, there is less input of the beam energy at a single point of location. Cutting speed of more than 750 mm/min did not contribute to reducing the HAZ. The trend of increasing HAZ on the top edge has been achieved with an increase in laser power. At higher power, a significant increase in the HAZ was observed for the untreated plate. Because higher laser power means higher heat energy, and it always affects the cutting edges. The mid-value of frequency and duty cycle leads to the lower HAZ. As gas pressure increased, less HAZ was achieved for the untreated plate because of easy removal of the melt from the kerf and did not allow it to resolidify on the edges. But for HT plate, gas pressure acts differently. Initially, HAZ decreased with an increase in the gas pressure, but at a higher gas pressure, HAZ increases. It may occur due to material composition and its hardness properties. A mathematical model for HAZ on the top edge has been developed with the determination coefficient of model R^2 was 98.8% and 99.5% for the untreated and HT plate, respectively, as shown in Eq. (5) and (6).

$$\begin{aligned}
 Y_{(HAZ\ top\ edge-Untreated)} &= -7.25 + 0.0036 X_1 - 8 \times 10^{-4} X_2 + 0.00056 X_3 + 0.14 X_4 + 24.5 X_5 - 1.48 \times 10^{-6} X_1^2 \\
 &+ 2.6 \times 10^{-7} X_2^2 - 4.3 \times 10^{-4} X_4^2 - 3 \times 10^{-7} X_1 X_2 - 2.76 \times 10^{-7} X_1 X_3 - 0.0064 X_1 X_5 \\
 &+ 1.7 \times 10^{-7} X_2 X_3 - 8.6 \times 10^{-6} X_2 X_4 + 0.0007 X_2 X_5 - 1.1 \times 10^{-5} X_3 X_4 + 0.002 X_3 \\
 &- 0.3 X_4 X_5
 \end{aligned} \tag{5}$$

$$\begin{aligned}
 Y_{(HAZ\ top\ edge-HT)} &= 13.1 + 0.005 X_1 - 1.2 \times 10^{-4} X_2 - 0.002 X_3 - 0.24 X_4 - 59.6 X_5 - 1.42 \times 10^{-6} X_1^2 \\
 &- 1.41 \times 10^{-7} X_2^2 - 4.48 \times 10^{-7} X_3^2 + 0.00088 X_4^2 + 161 X_5^2 - 5.74 \times 10^{-7} X_1 X_2 \\
 &- 2.67 \times 10^{-5} X_1 X_4 + 0.013 X_1 X_5 + 4.37 \times 10^{-8} X_2 X_3 + 1.64 \times 10^{-5} X_2 X_4 \\
 &+ 2.8 \times 10^{-5} X_3 X_4 + 0.0048 X_3 X_5 + 0.11 X_4 X_5
 \end{aligned} \tag{6}$$



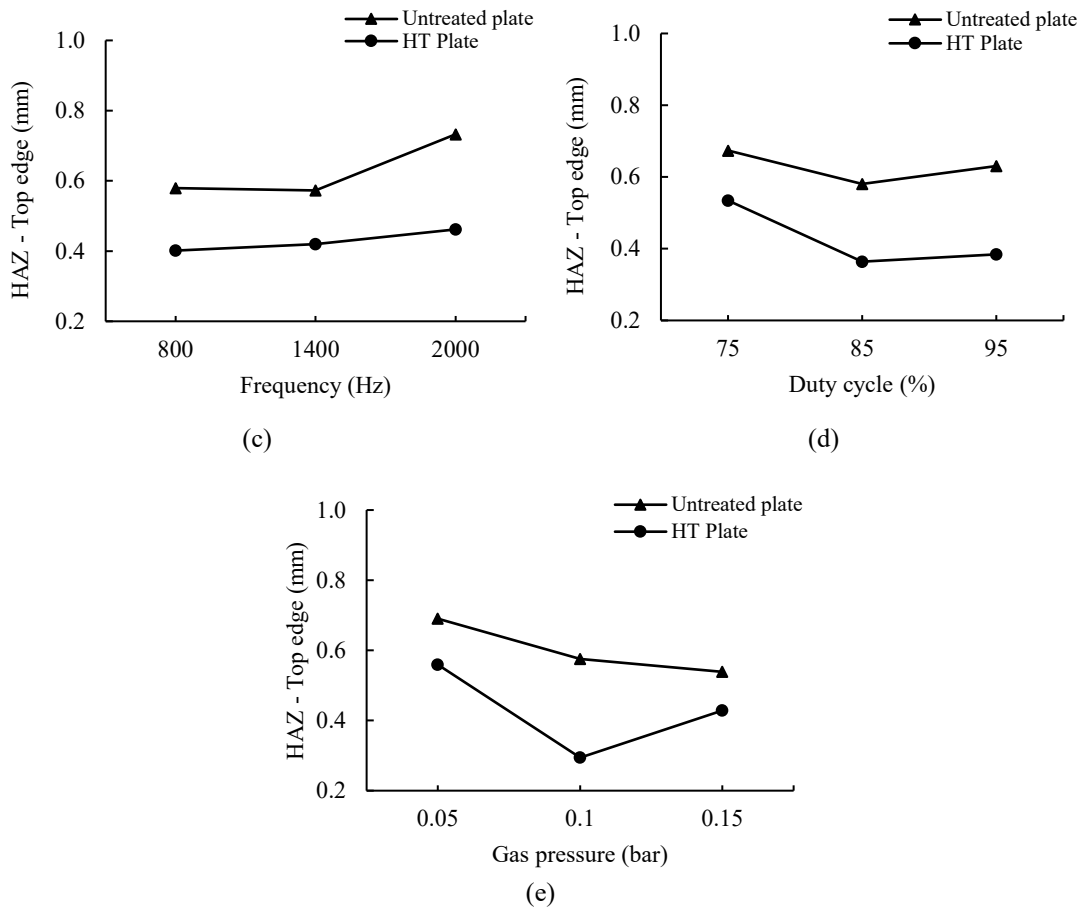
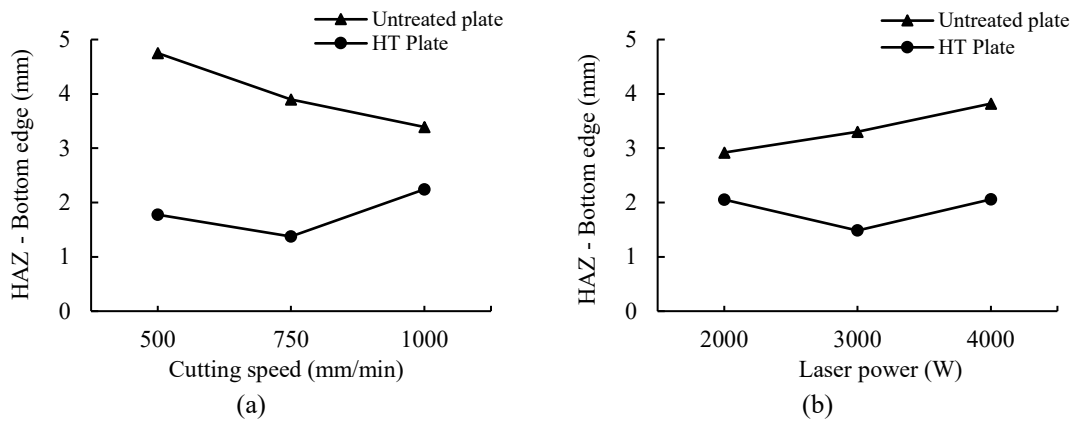


Figure 4. Main effect plot for top edge HAZ with respect to (a) cutting speed, (b) laser power, (c) frequency, (d) duty cycle and (e) gas pressure.

Figure 5 shows the main effect plot of the HAZ at bottom edge for both the plate. For the untreated plates, the same trends have been observed as per the plot of the top edge, but different trends achieved for HT plates. The mid-value of all the parameters gave minimum HAZ at HT plate may be due to material property and its hardness.



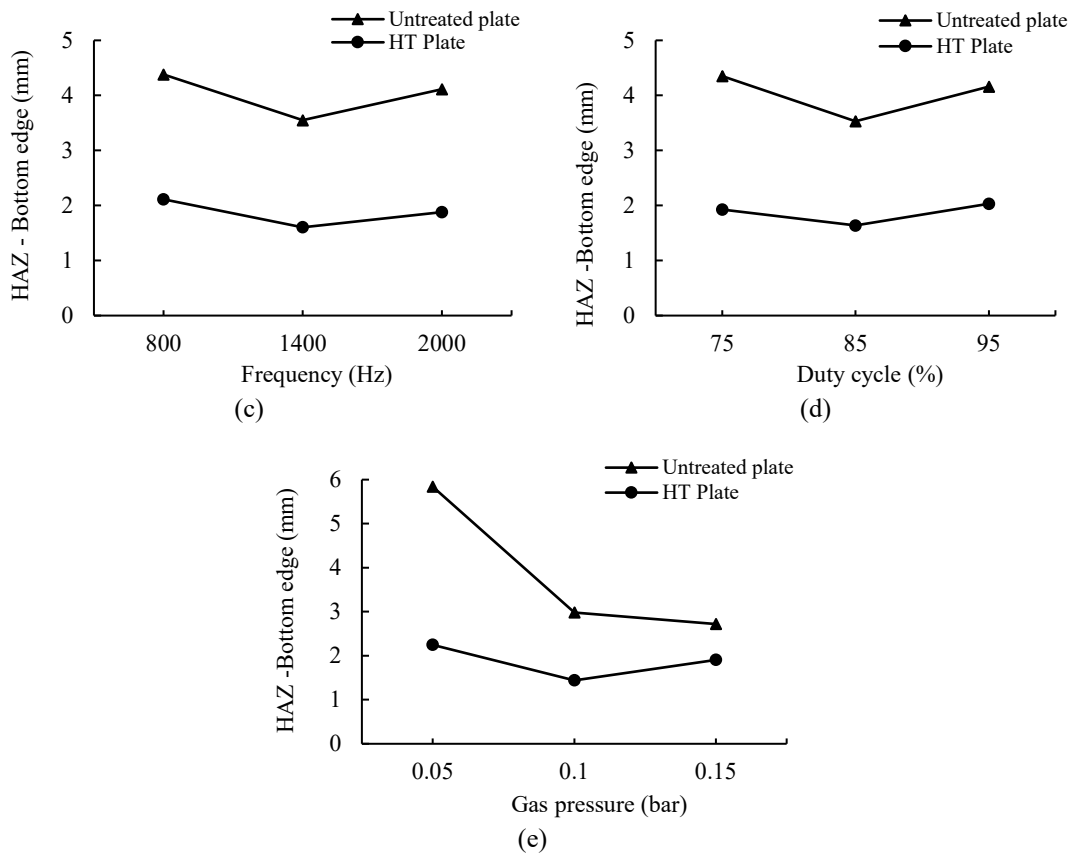
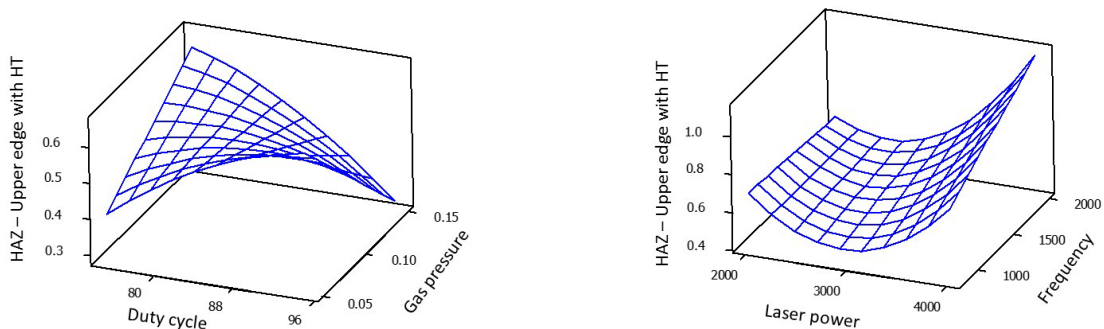


Figure 5. Main effect plot for bottom edge HAZ with respect to (a) cutting speed, (b) laser power, (c) frequency, (d) duty cycle and (e) gas pressure.

Figure 6 illustrates the response surface plot for HAZ upper edge to know the interaction effect. Figure 6(a) shows that higher gas pressure and duty cycle results in minimum HAZ on the upper edge. Figure 6(b) represents the lower frequency and mid-range of laser power leads to the minimum HAZ upper edge. A mathematical model for HAZ of the bottom edge has been developed with the determination coefficient of model R^2 was 96.9% and 97.1% for untreated and HT plate, respectively, as shown in Eq. (7) and (8).

$$\begin{aligned}
 Y_{(HAZ\ bottom\ edge-Untreated)} &= -13 - 0.01 X_1 - 0.0033 X_2 + 0.004 X_3 + 0.85 X_4 - 222 X_5 + 5.34 \times 10^{-7} X_2^2 \\
 &- 1.64 \times 10^{-6} X_3^2 - 0.0054 X_4^2 + 780 X_5^2 - 1.04 \times 10^{-6} X_1 X_2 + 8.85 \times 10^{-5} X_1 X_4 \\
 &+ 0.04 X_1 X_5 - 0.003 X_2 X_5
 \end{aligned} \tag{7}$$

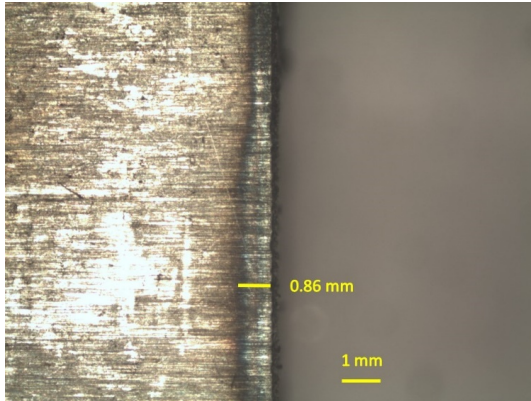
$$\begin{aligned}
 Y_{(HAZ\ bottom\ edge-HT)} &= -14 + 0.0016 X_1 - 0.002 X_2 - 0.0037 X_3 + 0.49 X_4 - 11.5 X_5 - 4.17 \times 10^{-7} X_2^2 \\
 &- 3.26 \times 10^{-7} X_3^2 - 0.0027 X_4^2 + 247 X_5^2 - 4.5 \times 10^{-7} X_1 X_2 + 1.03 \times 10^{-6} X_1 X_3 \\
 &- 0.008 X_1 X_5 + 7.08 \times 10^{-8} X_2 X_3 - 6.75 \times 10^{-6} X_2 X_4 + 0.0029 X_2 X_5 + 3.87 \times 10^{-5} X_3 X_4 \\
 &+ 0.0017 X_3 X_5 - 0.54 X_4 X_5
 \end{aligned} \tag{8}$$



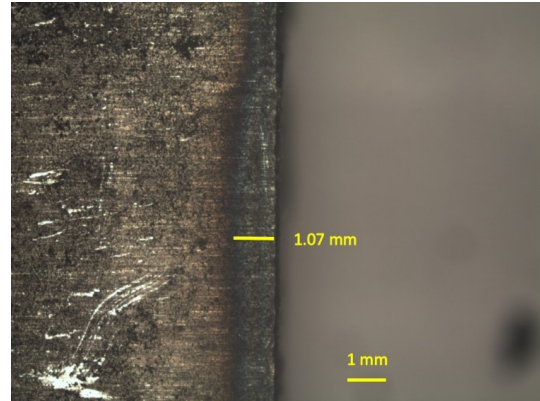
(a) Response surface plot for duty cycle and gas pressure (b) Response surface plot for laser power and frequency

Figure 6. Response surface plot for HAZ upper edge.

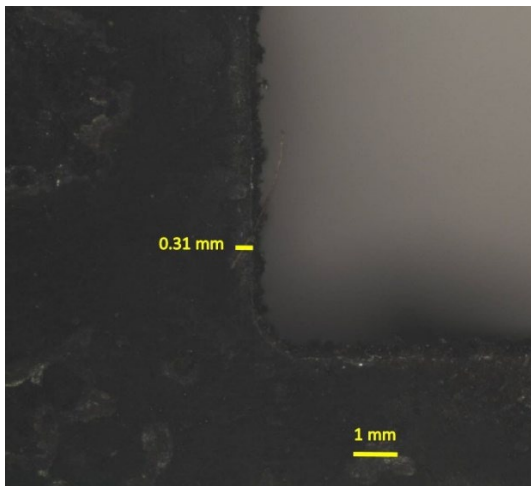
The top and bottom cutting edges observed under a 3D microscope, and the image for one hole is shown in Figure 7 with greater magnification. The HAZ on the bottom edge for the untreated plate was visible through naked eyes. The bottom edge of the HT plate can be distinguished with two layers of HAZ; one is with the white area, and another layer observed may be a cause of resolidification of molten metal.



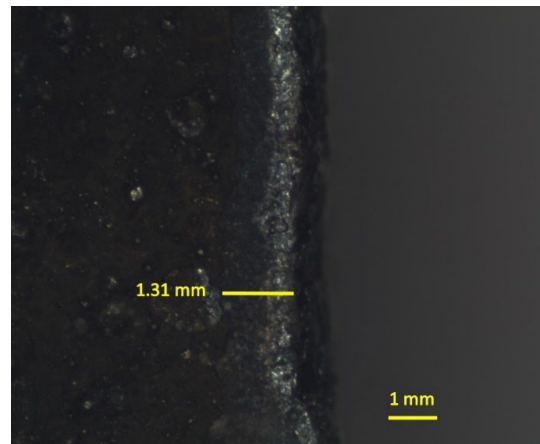
(a) Top edge HAZ showed for an untreated plate at 2.5× zoom



(b) Top edge showed for an untreated plate at 2.5× zoom



(c) Top edge HAZ showed for an HT plate at 3× zoom



(d) Bottom edge HAZ showed for an HT plate at 4× zoom

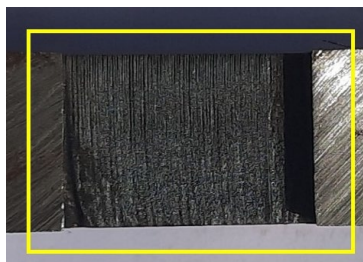
Figure 7. HAZ captured using a 3D microscope at 2.5×, 3×, and 4× magnification.

Effect of Process Parameters on Surface Roughness

Cutting edges have been noticed to understand the striation pattern and visible effect of parameters on the quality of the holes, as shown in Figure 8. Striations were present in each cut surface and observed with some remarkable patterns. Also, it has been noticed that the higher cutting speed leads to a less striation surface. Corners of the few holes were observed with some visible damages because of a paused moment of the laser beam to change the direction or axis of its travel.



(a) Cut front section of a 14 mm untreated plate



(b) Cut front section of a 14 mm HT plate



(c) Damages of corner edge in a few holes

Figure 8. Hole cut section for an untreated and HT plate.

Surface roughness is the prime component to evaluate the cut quality. It is a tough and necessary task for the die industry to achieve better surface roughness for hard and thick material. Figure 9 shows the main effect plot of surface roughness concerning all process parameters. At the higher cutting speed, better surface roughness achieved due to less concentration of the heat energy at one point; hence less striation achieved. A minor increment in the surface roughness was observed in the untreated plate with an increase in the laser power. Because higher power deals with the higher heat energy, it increases the penetration of heat and damages the kerf edges. For HT plate, very low and high power leads to higher surface roughness; it might occur due to insufficient or excess heat energy generated for the cutting of the hole. From the main effect plot, the frequency and duty cycle were not much significant. But, for achieving good surface roughness, these machine parameters must be set at their mid position. In a general way, higher gas pressure helps to extract the melt from the kerf and results in better surface roughness. But here, gas pressure damages the cutting edges as flow became turbulent at higher gas pressure.

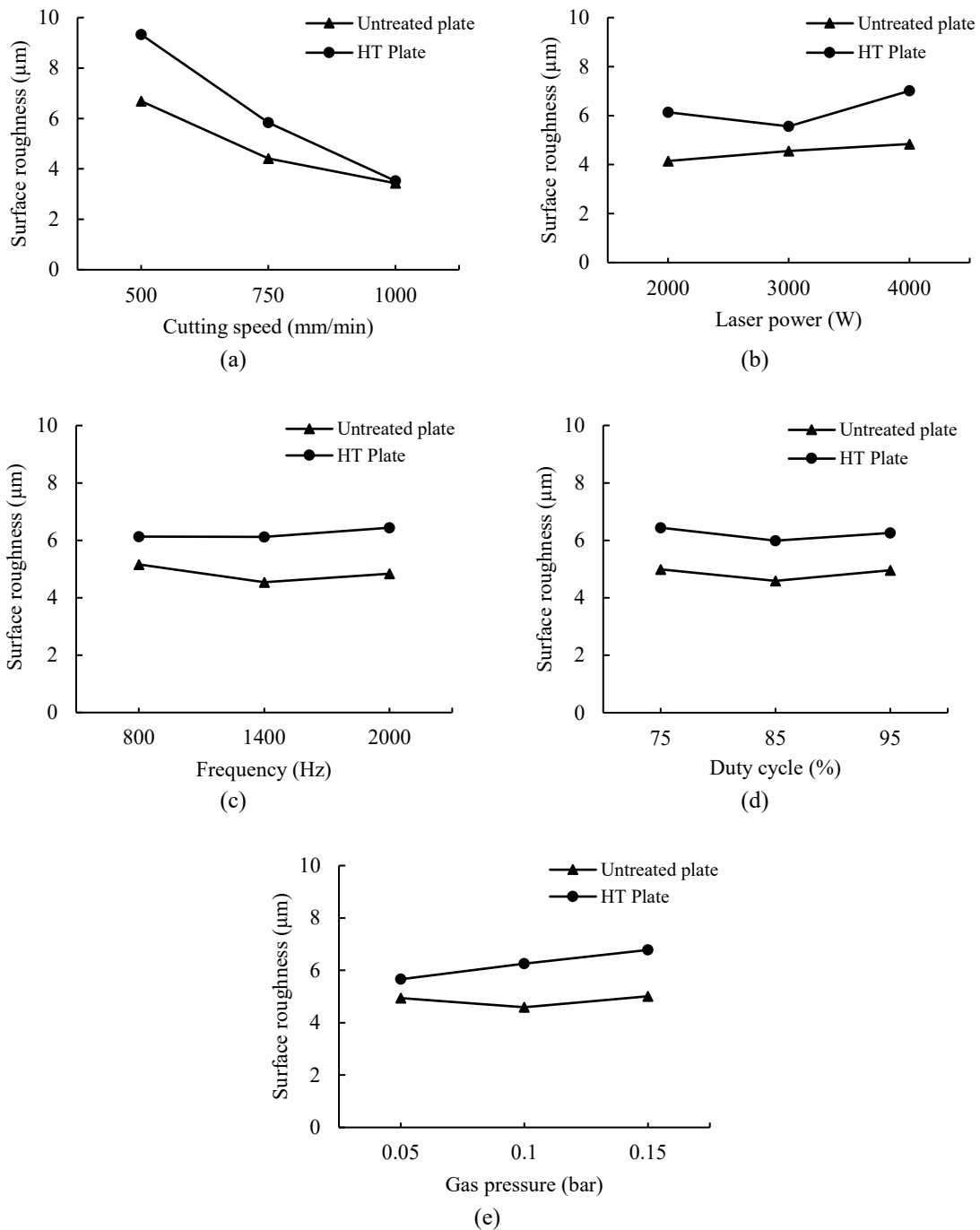


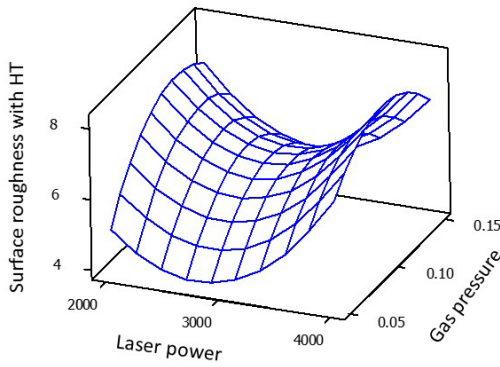
Figure 9. Main effect plot for surface roughness concerning (a) cutting speed, (b) laser power, (c) frequency, (d) duty cycle and (e) gas pressure.

Figure 10 illustrates the response surface plot for surface roughness to understand the interaction effect of process parameters. Figure 10(a) represents that lower gas pressure and mid-range of laser power leads to better surface roughness. Figure 10(b) shows a lower duty cycle and higher laser power leads to the minimum roughness. A mathematical model

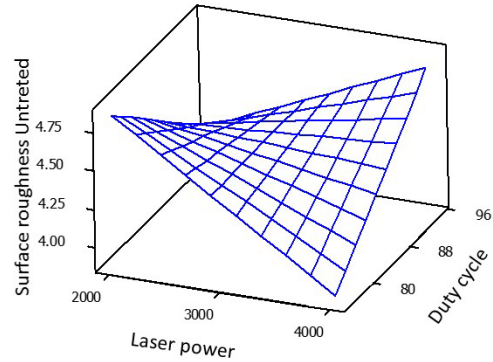
for surface roughness has been developed with a coefficient of the determination of the model R^2 was 97.3% and 95% for untreated and HT plate respectively and shown in Eq. (9) and (10).

$$Y_{(Ra-Untreated)} = 20.2 - 9.54 \times 10^{-4} X_1 - 0.003 X_2 - 0.0047 X_3 - 0.11 X_4 + 0.62 X_5 + 1.03 \times 10^{-5} X_1^2 - 1.43 \times 10^{-6} X_1 X_2 - 1.78 \times 10^{-6} X_1 X_3 - 1.67 \times 10^{-4} X_1 X_4 + 4.65 \times 10^{-5} X_2 X_4 + 6.81 \times 10^{-5} X_3 X_4 \tag{9}$$

$$Y_{(Ra-HT)} = 20.7 - 0.026 X_1 - 0.01 X_2 + 0.0048 X_3 - 0.016 X_4 + 209 X_5 + 9.5 \times 10^{-6} X_1^2 + 1.88 \times 10^{-6} X_2^2 - 1.85 \times 10^{-6} X_3^2 - 492 X_5^2 - 1.07 \times 10^{-6} X_1 X_2 - 2.3 \times 10^{-6} X_1 X_3 + 0.0001 X_1 X_4 - 0.024 X_1 X_5 + 5.23 \times 10^{-7} X_2 X_3 - 0.009 X_2 X_5 + 0.008 X_3 X_5 - 0.77 X_4 X_5 \tag{10}$$



(a) Response surface plot for surface roughness, laser power and gas pressure



(b) Response surface plot for surface roughness, laser power and duty cycle

Figure 10. Response surface plot for surface roughness.

Optimisation and Significant Parameters

A relationship between the process parameters and responses have been determined using the empirical mathematical models and compared and analysed with the experimental results. A comparison seems that the model is best suited to the experimental value. By using the DOE, a significant contribution for individual, square, and interaction effect of parameters have been carried out at a 95% confidence level and probability coefficient, $p < 0.001$ value and documented in Table 5.

Table 5. Significant process parameter for all the responses.

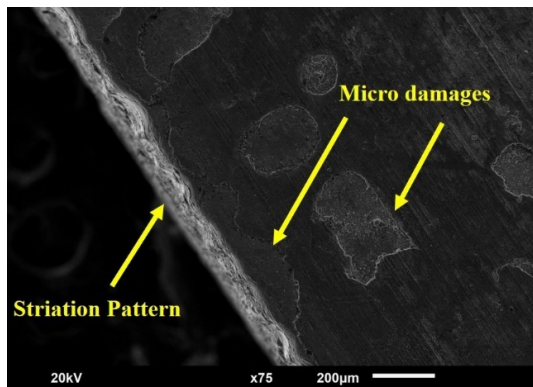
Response	Type of plate	Individual effect	Square effect	Interaction effect
Taper effect	Untreated	Cutting speed, laser power, gas pressure	Cutting speed	Cutting speed * gas pressure
	HT	Gas pressure	Gas pressure	Laser power * gas pressure, Cutting speed * frequency, Laser power * duty cycle
HAZ (top edge)	Untreated	Cutting speed, laser power, frequency	Laser power	Cutting speed * laser power, Cutting speed * gas pressure, Laser power * frequency, Laser power * duty cycle, Duty cycle * gas pressure
	HT	Cutting speed, duty cycle, gas pressure	Frequency, gas pressure	Cutting speed * laser power, Cutting speed * duty cycle, Cutting speed * gas pressure, Laser power * duty cycle, Frequency * duty cycle, Frequency * gas pressure
HAZ (bottom edge)	Untreated	Cutting speed, laser power, gas pressure	Gas pressure	Cutting speed * gas pressure
	HT	Cutting speed	Gas pressure	Duty cycle * gas pressure, Frequency * duty cycle
Surface roughness	Untreated	Cutting speed	Cutting speed	Cutting speed * duty cycle, Laser power * duty cycle, Frequency * duty cycle
	HT	Cutting speed, laser power, gas pressure	Laser power, gas pressure	Laser power * gas pressure

The optimised value of process parameters has been derived using DOE and statistical software. Then confirmatory tests were carried out to validate the adequacy of the mathematical model. The difference between these two results is given in Table 6.

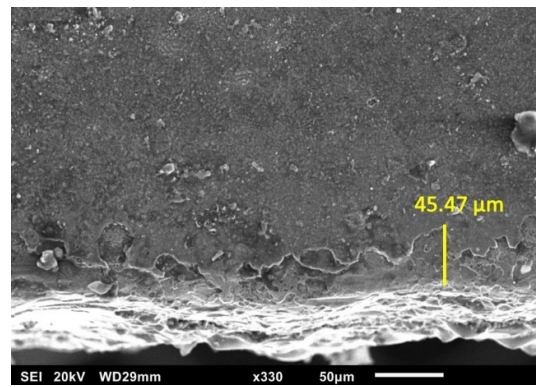
Table 6. Confirmatory test at an optimised process parameter and their results.

Response	Type of plate	X1	X2	X3	X4	X5	Model value	Experimental	Difference (%)
Taper angle	Untreated	500	4000	2000	76	0.15	0.065	0.067	2.98
	HT	798	2505	800	95	0.12	0.51	0.57	10.24
HAZ (Top)	Untreated	500	2686	800	75	0.05	0.209	0.23	9.14
	HT	500	2000	800	95	0.12	0.09	0.1	10
HAZ (Bottom)	Untreated	1000	3717	2000	75	0.11	0.935	1.03	9.21
	HT	500	2768	2000	75	0.09	0.2	0.22	7.74
Ra	Untreated	1000	4000	2000	75	0.05	2.03	2.11	3.8
	HT	1000	2747	2000	75	0.05	0.25	0.27	7.25

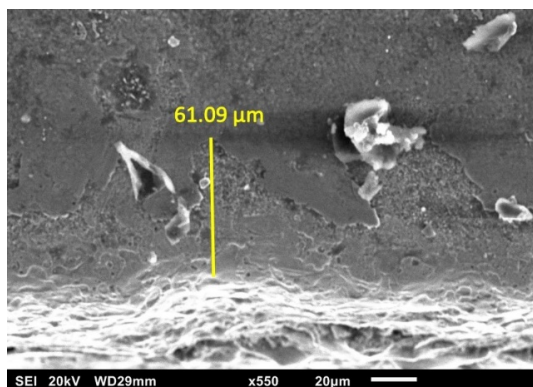
SEM has been used to understand and analysed the defect of cutting edges. Figure 11 shows the scanning electron microscopic images nearby the cutting edges of understanding the surface damages and cracks generated in microns. Specimen size has been kept 10 mm in length. Care has been taken to prevent the specimen from surface oxidation due to moisture in the atmosphere. The top edge after cutting the holes has been found alright by the naked eye observation, but through SEM, the exact damages have been observed. Small microcracks were observed at the top edge of the cut section. Thermal damages due to oxygen gas, higher beam velocity, or resolidification of the melt cause the micro-cracks on the surface. Side by side burning of cutting edges generate the striations, and striation patterns were studied using SEM images. An increase in laser power leads to an increase in the striation because higher laser beam energy creates an influence on the cutting edges. Figure 11 shows the sample photographs of cutting edges which exhibit the striation pattern and micro-cracks nearby the cutting edges.



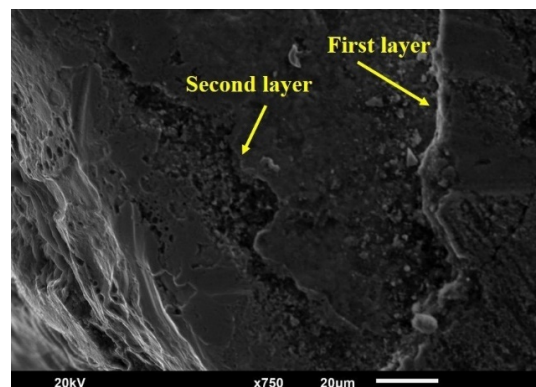
(a) Striation pattern at 75× zoom and minor damages on the top edge



(b) Microcracks at top edges of an untreated plate at 330× zoom



(c) Microcracks on top edges of HT plate at 550× zoom



(d) Two layers of microcracks at top edges at 750× zoom

Figure 11. SEM images with striation pattern and micro damages/cracks near cut edges.

CONCLUSION

The process parameter of CO₂ laser cutting for 14 mm thick die alloy steel EN-31 was analysed experimentally and statistically. This research aimed to achieve a minimum taper angle, minimum HAZ at top and bottom edge, and better surface roughness for a difficult to cut and thick plate. Quadratic relation has been generated for each response and found better adequacy with the experimental results. Optimum parameters were identified using statistical software and validated its mathematical results with experiments. Using DOE, the significance of the parameter's individual, square, and interaction effect has been tabulated.

It is quite impossible to achieve a zero-taper angle for hard and thick material. For untreated plate, cutting speed, laser power, and gas pressure were the significant parameters to control the taper angle. The mid-value of all the parameters leads to the minimum taper angle for the HT plate. The taper angles of 0.067° and 0.57° were achieved for the untreated and HT plates, respectively, when the parameters optimised.

The HAZ on the top and bottom edge for both plates has been studied in a separate main effect plot. Because of the large amount of heat-conduction and melt extracted from the bottom, the bottom edge has a higher HAZ compared to the top edge. Also, the untreated plates observed have a higher HAZ than the HT plate; may be due to the resolidification of the melt. Higher cutting speed, low laser power, and higher gas pressure cause the minimum HAZ for an untreated plate. Minimum HAZ achieved for HT plate if all the parameters set to their middle position. At the optimised level, minimum HAZ (i.e. 0.23 mm and 0.1 mm) observed at the upper edge; and (1.03 mm and 0.22 mm) at the lower edge for the untreated and HT plates, respectively.

A cutting speed is the most significant parameter to achieve better surface roughness and less striation. Visual inspection was carried out at the hole's cross-section to understand the striation pattern, resolidified layer, and corner qualities. Striation pattern and damage of the surface near the cutting edge were observed using SEM. The surface quality for a few holes couldn't be achieved as expected as improper penetration of laser beam not able to cut the through-hole. The surface roughness of 2.11 µm and 0.27 µm have been achieved at an optimised set of parameters for untreated and HT plates, respectively. An acceptable cutting quality has been achieved with the optimum set of parameters, and it can be considered as a useful research contribution to the die industry for cutting thick and difficult to cut die steel material.

ACKNOWLEDGEMENT

The authors acknowledge Charotar University of Science and Technology for providing instrumental facilities for the measurement and analysis and the Prashant Group of Companies for providing a platform for experimentation.

REFERENCES

- [1] Chatterjee S. A review of: Non traditional machining process by Weller EJ. 2nd ed. American Society of Tool & Manufacturing Engineers; 1984. *Materials and Manufacturing Processes* 1990; 5(1): 139–140.
- [2] Dahotre NB. Laser material processing by Steen WM, London: Springer-Verlag; 1991. *Materials and Manufacturing Processes*, 1993; 8(3): 399–400.
- [3] Powell J. CO₂ Laser cutting. 2nd ed. London: Springer; 1998.
- [4] Moradi M, Moghadam MK, Shamsborhan M, et al. Post-processing of FDM 3D-printed polylactic acid parts by laser beam cutting. *Polymers* 2020; 12(3): 550.
- [5] Lee CM, Woo WS, Baek JT, Kim EJ. Laser and arc manufacturing processes: A review. *International Journal of Precision Engineering and Manufacturing* 2016; 17(7): 973–985.
- [6] Zhou Y. A review on fiber laser striation-free cutting for thick section stainless steel. In: *International Symposium on Optoelectronic Technology and Application*, Beijing, China; 13-15 May, 2014.
- [7] Sharma A, Yadav V. Experimental analysis of Nd-YAG laser cutting of sheet materials – A review. *Optics and Laser Technology* 2018; 98: 264–280.
- [8] Ahmed N, Rafaqat M, Pervaiz S, et al. Controlling the material removal and roughness of Inconel 718 in laser machining. *Materials and Manufacturing Processes* 2019; 34(10): 1169–1181.
- [9] Orishich AM, Malikov AG, Shulyatyev VB, Golyshev AA. Experimental comparison of laser cutting of steel with fiber and CO₂ lasers on the basis of minimal roughness. *Physics Procedia* 2014; 56: 875–884.
- [10] Zlamal T, Malotova S, Petru J, et al. The evaluation of the surface quality after laser cutting. *MATEC Web Conference* 2018; 244:02009.
- [11] Kangal AM, Uysal A. Analysing optimum process parameters in laser cutting of EN10025-2 steel plate. *Journal of Advances in Manufacturing Engineering* 2020; 1(1): 23–28.
- [12] Mahamani A, Chakravarthy A. Investigation on laser drilling of AA6061-TiB₂/ZrB₂ in situ composites. *Materials and Manufacturing Processes* 2017; 32(15): 1700–1706.
- [13] Gao W, Lei M, Li B, et al. Investigations on the laser cutting of LiNbO₃. *Optik* 2020; 201: 163508.
- [14] Rao S, Sethi A, Das A, et al. Fibre laser cutting of CFRP composites and optimisation of process parameters through response surface methodology. *Materials and Manufacturing Processes* 2017; 32 (14): 1612–1621.

- [15] Moghadasi K, Tamrin B, Fikri K. Experimental investigation and parameter optimisation of low power CO₂ laser cutting of a carbon/kevlar fibre-reinforced hybrid composite. *Lasers in Engineering* 2019; 45(1-3): 85-108.
- [16] Molian PA. Dual-beam CO₂ laser cutting of thick metallic materials. *Journal of Materials Science* 1993; 28: 1738-1748.
- [17] Mushtaq RT, Wang Y, Rehman M, et al. State-of-the-art and trends in CO₂ laser cutting of polymeric materials - A review. *Materials* 2020; 13: 3839.
- [18] Golyshev AA, Orishich AM, Shulyatyev VB. Effect of the laser beam polarisation state on the laser cut surface quality. In: *Lasers in Manufacturing Conference, German Scientific Laser Society (WLT), Munich, Germany; 22-25 June, 2015*.
- [19] Hossain A, Hossain A, Nukman Y, et al. A fuzzy logic based prediction model for kerf width in laser beam machining. *Materials and Manufacturing Processes* 2015; 31: 679-684.
- [20] Seong YO, Shin JS, Kim TS, et al. Effect of nozzle types on the laser cutting performance for 60 mm thick stainless steel. *Optics and Laser Technology* 2019; 119: 105607.
- [21] Genna S, Menna E, Rubino G, Tagliaferri V. Experimental investigation of industrial laser cutting: The effect of the material selection and the process parameters on the kerf quality. *Applied Sciences* 2020; 10: 49-56.
- [22] Moradi M, Abdollahi H. Statistical modelling and optimisation of the laser percussion micro drilling of thin sheet stainless steel. *Lasers in Engineering* 2018; 40(4-6): 375-393.
- [23] Lawrence J, Li L. The challenges ahead for laser macro, micro and nano manufacturing. In: *Advances in Laser Materials Processing*. 2nd ed. Elsevier BV, 2018, p 23-42.
- [24] Tahir AFM, Rashid AR, Sariff NE, Rahim EA. CO₂ laser cutting performance on ultra high strength steel (UHSS). *Lasers in Manufacturing and Materials Processing* 2020; 7: 15-37.
- [25] Haddadi E, Moradi M, Ghavidel AK, et al. Experimental and parametric evaluation of cut quality characteristics in CO₂ laser cutting of polystyrene. *Optik* 2019, 184: 103-114.
- [26] Montgomery DC. *Design and analysis of experiments*. 2nd ed. New York: John Wiley & Sons; 1984.
- [27] Khuri AI, Cornell JA. *Response surfaces design and analysis*. 2nd ed. New York: Marcel Dekker; 1996.